

EAGLE - ENVIRONMENT FOR AUTONOMOUS GNC LANDING EXPERIMENTS

M. Dumke⁽¹⁾, M. Sagliano⁽¹⁾, P. Saranrittichai⁽¹⁾, G. F. Trigo⁽¹⁾, S. Theil⁽¹⁾

⁽¹⁾ German Aerospace Center, Institute of Space Systems, Robert-Hooke-Str. 7, 28359 Bremen, Germany, +49-421-244201262, michael.dumke@dlr.de

ABSTRACT

Precise landing on planets, moons and other larger celestial bodies requires powered descent, hovering, and vertical landing. Similarly, recent and future concepts for Re-usable Launch Vehicles (RLVs) also involve a vertical take-off and landing. The development of Guidance, Navigation, and Control (GNC) for this type of vehicles is a challenging task. To support this, a Vertical Take-Off and Landing (VTOL) vehicle has been developed for demonstrating the capability of conducting soft landings, smooth ascent, and hovering.

The focus was put on a platform for testing new and advanced GNC algorithms that employ a base set of sensors and actuators typically present on such vehicles. It should represent a dynamics similar to a thrust vector controlled planetary lander or RLV, and should allow fast turn-around times as well as rapid prototyping capabilities for testing. Additionally, the platform should provide the option for an additional small payload, e. g., enhancing the on-board avionics with different or more precise sensors.

The result of this platform development is EAGLE (Environment for Autonomous GNC Landing Experiments). Its lift-of-mass is about 30 kg and it is powered by a jet engine with a maximum thrust of 400 N.

1 INTRODUCTION

Recent and future missions target precise descent and landing. This can be on one the hand the powered descent and landing of a re-usable first stage of a launch vehicle as it was demonstrated several times by SpaceX with its Falcon 9 launch system. On the other hand, precise descent and landing has been applied to planetary missions and is foreseen for many more future missions to Mars and Moon. The development of Guidance, Navigation, and Control (GNC) techniques for these applications remains a challenging task although several mission have been already successfully completed. Especially in Europe, the experience in this field of GNC is worth an improvement.

Several ideas to support and accelerate the GNC development using demonstrators have been conceived in the past in Europe. Only a very few have been implemented like the HOMER demonstrator of Airbus Defense and Space [2, 3]. Many of these ideas got halted due to the high cost and high complexity of an experimental vehicle using rocket engines for the main thrust. The issue of handling explosive or toxic materials in an experimental vehicle creates high costs and limits flexibility and turn-around time. In order to decouple the high complexity of rocket propulsion from the GNC development the experimental Vertical Take-Off and Landing (VTOL) vehicle EAGLE (Environment for



Figure 1: The experimental VTOL vehicle EAGLE (left) and its ancestor NASA's Lunar Landing Training Vehicle (LLTV) of the Apollo program¹(right)

Autonomous GNC Landing Experiments) was conceived. The idea is based on NASA's Lunar Landing Training Vehicle (LLTV) of the Apollo program which was used to train the pilots of the lunar landing vehicles (LLV). Both vehicles are shown in Figure 1.

The main goal of EAGLE is to provide dynamics, sensors and actuators similar to a landing vehicle. For most applications existing, this include a vertical main thruster with thrust vector control and a Reaction Control System (RCS). Compared to the LLTV there is one major difference: The LLTV was designed to create environment and dynamics similar to the lunar landing environment. For that reason it was using a part of the main thrust for gravity compensation and the vehicle attitude was decoupled from the main thrust direction. This way it was achieved that the pilot's "feeling" when flying the LLTV was very close to the real LLV on the Moon. Since the goal of EAGLE is to "train" GNC software, the gravity compensation can be omitted due to the fact that we can program the GNC software what gravity to expect on Earth or on the Moon and to consider this in the GNC algorithms and software.

Based on the needs for simple handling, similar flight dynamics, high flexibility, and fast turn-around times, a small VTOL vehicle with a jet engine as main thruster was developed. This paper will provide in Section 2 an overview of the system. The following two sections will provide information about the on-board hybrid navigation system and the control system. This is followed by a presentation of flight results in Section 5. Finally, some conclusions are drawn and further steps and developments are sketched.

2 EAGLE SYSTEM OVERVIEW

The most apparent features of EAGLE, see Figure 2a, are the landing legs and the main structure centrally housing the main engine. The main engine is a one stage jet engine capable of lifting the roughly 30 kg wet-mass of the lander. The landing gear absorbs the landing shocks protecting the sensitive electronics, payloads, and the structure itself.

The light-weight main structure of EAGLE is build from five aluminum sandwich parts interconnected with aluminum brackets and clamps. Figure 2b shows the two rings that are linked with three

¹Source: Great Images in NASA; Image #: ECN-506; Date: 01/01/1964

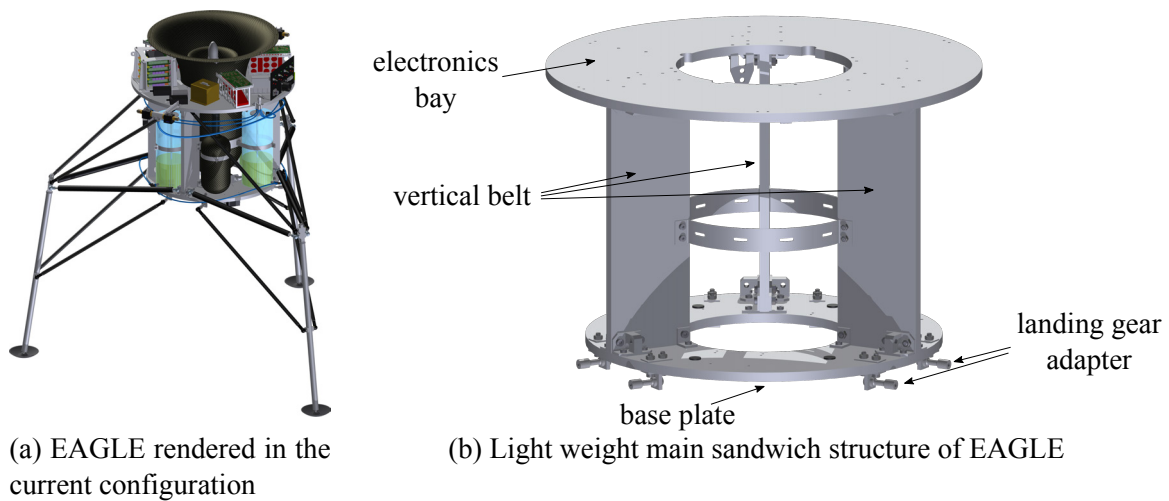


Figure 2: Configuration and structure of EAGLE

(identical) vertical belts. The upper ring is the *electronics bay*, that houses the overall avionics of the lander, and the *base plate* closes the middle section for the fuel and gas tanks.

The central cutaway is reserved for the main engine and the Thrust Vector Control (TVC) system that deflects the exhaust stream of the engine.

Figure 3 shows the landing gear system in fully extended and fully retracted configurations. Each leg is connected by four carbon rods supported with joints on each side. Additionally, each leg is held by two gas dampers in the extended position (Figure 3 (left)) in order to absorb shocks and forces during landing (Figure 3 (right)).

2.1 Actuation

Three actuation systems are integrated on the lander. First of all, a jet engine (Section 2.1.1) generates the main thrust by commanding the fuel flow into the jet engine's burning chamber. Secondly, a

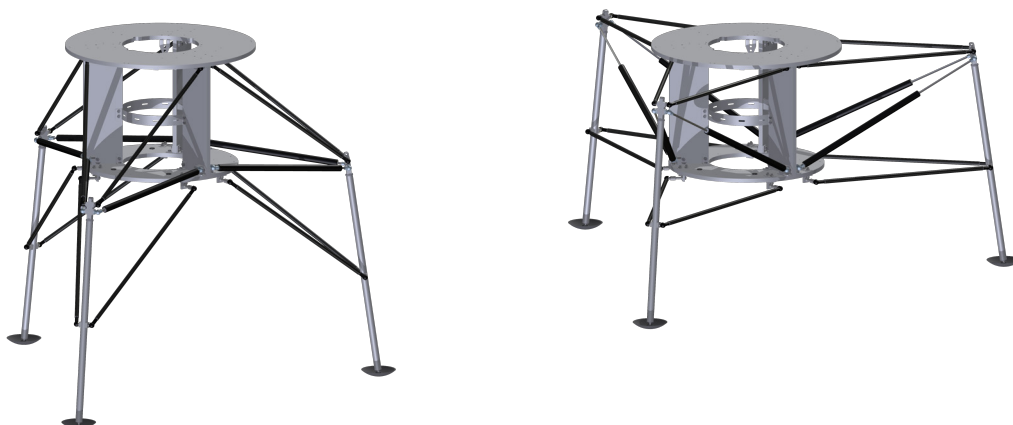


Figure 3: Landing gear system of EAGLE

Thrust Vector Control system (Section 2.1.2) employing two vanes aligned perpendicular to each other deflects the thrust for *pitch* and *yaw* maneuvers². And last, a Reaction Control System (Section 2.1.3) using a cold-gas thruster set.

2.1.1 Jet engine and fueling system

The jet engine generates the main thrust that acts against the gravitational force and accelerates the vehicle. Its maximum nominal static thrust is around 400 N at sea level. At this point the one-stage-radial compressor (and the one-stage turbine) rotates at approximately 100 000 RPM. The only command necessary to control the engine is the pump voltage level. This is issued to the Electronic Control Unit (ECU) which provides the commanded voltage to the fuel pump. In return, the ECU provides housekeeping data for monitoring the complex jet engine system.

The whole engine and fueling system is depicted in Figure 4. Centrally within the set-up is the compact engine with the inlet on the upper end and the exhaust nozzle on the lower end. This is surrounded by four 1.8 l kerosene tanks all interconnected to allow equalizing of their filling level.

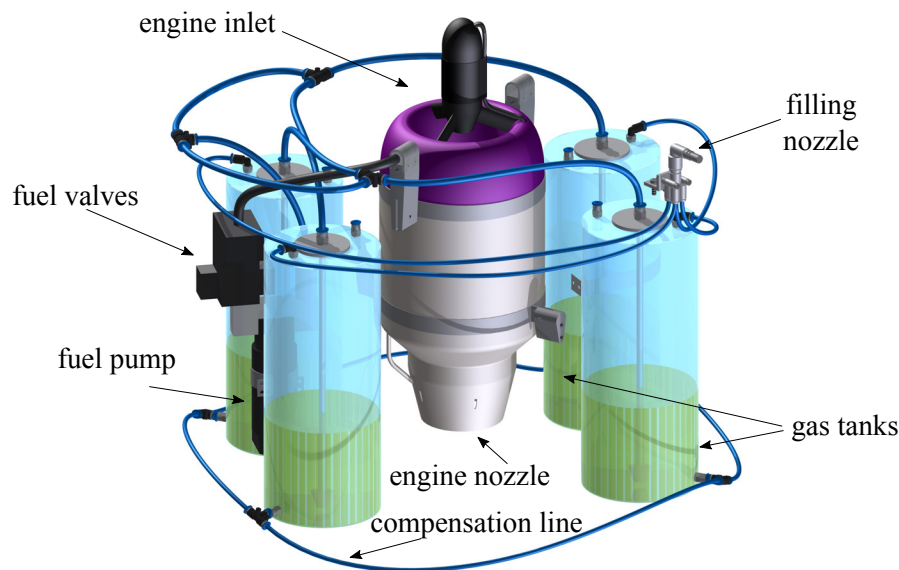


Figure 4: EAGLE's main engine and fueling system

2.1.2 Thrust Vector Control System

For controlling the attitude around EAGLE's pitch and yaw axes a TVC system was placed on the lower side of the main structure. Figure 5 shows the main components that constitute this system. Each control motor rotates a shaft connected to a vane. The deflection range for each vane is about ± 12 deg. Higher angles are not possible due to the "v"-shaped cutouts on the vanes where the perpendicular axes cross. Each vane is supported by two ceramic ball bearings able to withstand the high temperature of the jet engine's exhaust stream.

²Like a launch vehicle the *roll* axis points upwards in the main flight direction.

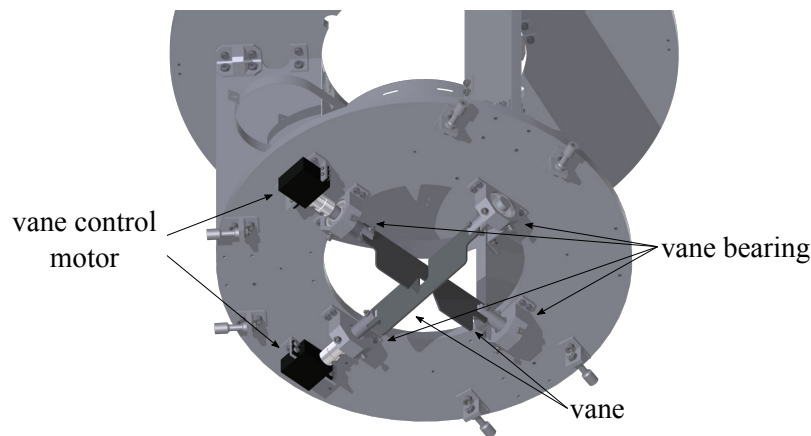


Figure 5: Thrust Vector Control system of EAGLE

The effectiveness of the system is highly dependent on that of main thrust. Tests with a thrust of about 270 N showed lateral forces of about ± 30 N at maximum vane deflection angles.

2.1.3 Roll Control system

Figure 6 depicts the Reaction Control System used for the roll control of EAGLE. The actuators that generate the control forces are connected to the front and back lever arms and consist of electromagnetic on/off valves and nozzles. The valves are fed pressurized air by a hose connected to the pressure regulators.

The tanks hold 1.1 l at 300 bar when full. The pressure is reduced by a two-stage system down to 12.5 bar. The nozzle is attached to the valve with a design optimized for a nominal control thrust of 4 N.

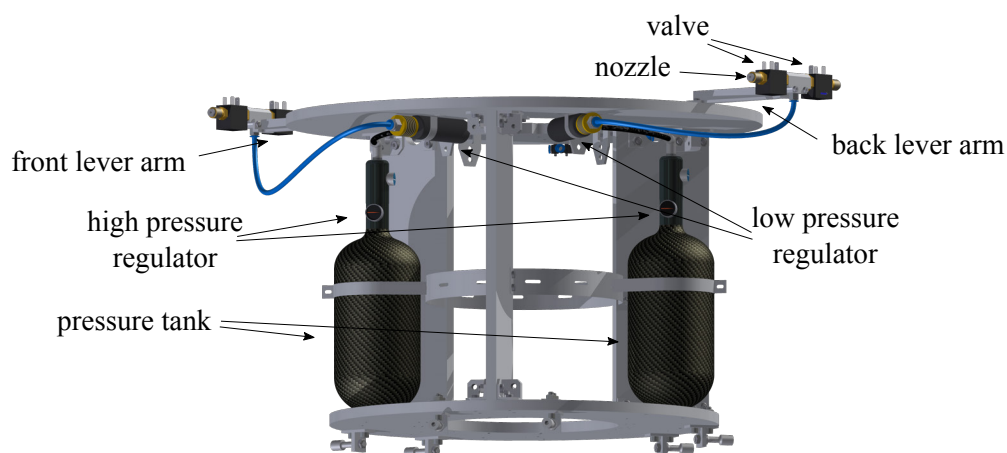


Figure 6: Cold-gas-based Reaction Control System for the roll axis

2.2 Avionics and Software

Figure 7 shows a schematic of the avionics on board of EAGLE. The main element is the On-board computer (OBC) which has (indirect) access to all available sensors and actuators. Depending on the electrical interface of a device it is either connected directly to the OBC, or the data stream is routed via an *Interface Board* that provides access to low-level interfaces (SPI, I²C, PWM, etc.).

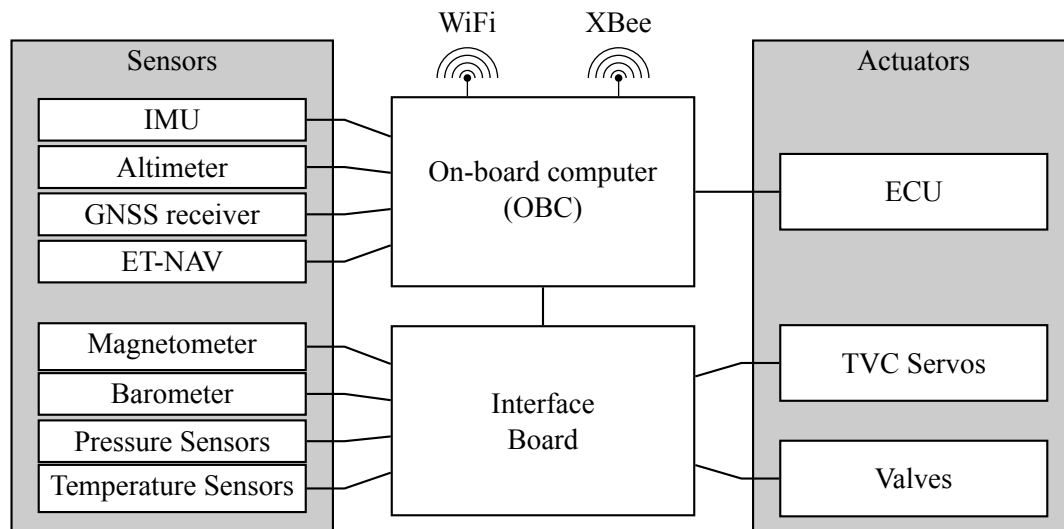


Figure 7: Avionics overview of EAGLE

Communication with the ground station is guaranteed via two different wireless links on two different frequency bands (WiFi and XBee). In case of a disrupted WiFi link, the low bandwidth interface to EAGLE via XBee is still available. This allows commanding emergency landings or monitoring the most important housekeeping data.

The OBC runs the real-time operating system *QNX* which executes the on-board software including the Guidance, Navigation, and Control algorithms. The main software system is built from a MATLAB/Simulink model. *Simulink Coder* generates “C” code from this model that is cross-compiled for the OBC. This enables a rapid prototyping functionality allowing quick software changes in between tests and directly using developed and tested Simulink algorithms without the necessity of porting the algorithm to the target platform.

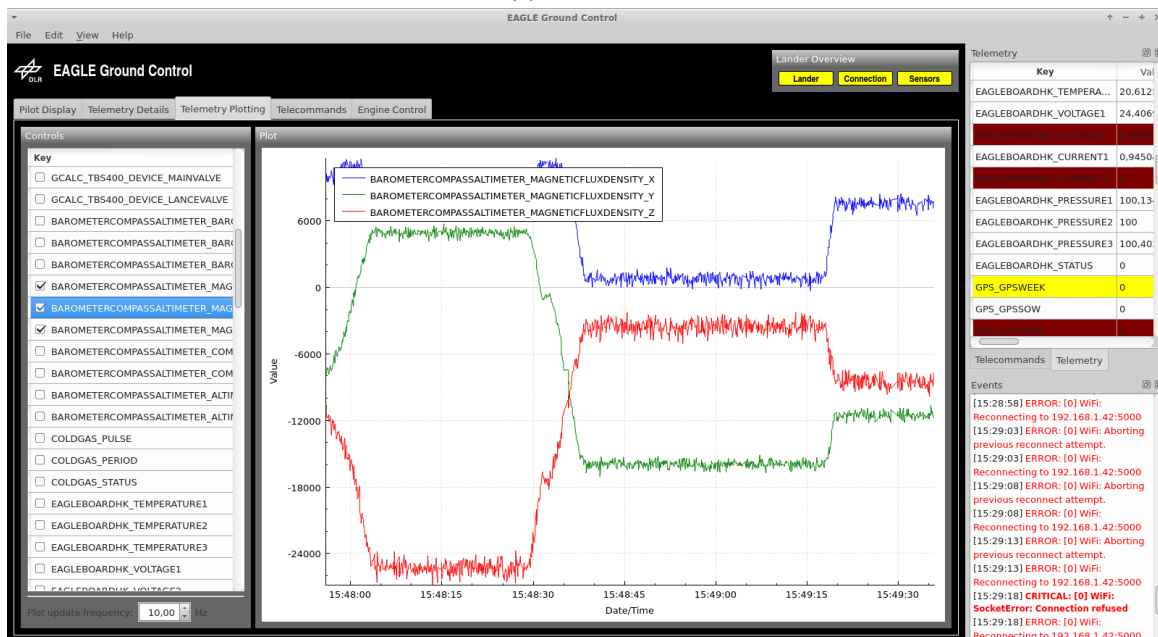
A real-time interface transmits the Telemetry/Telecommand (TM/TC) data between EAGLE and ground station computer. This interface serves the two wireless links that are present on EAGLE, transparently providing the telemetry data to the user from both communication channels. Additional telemetry or command parameters can be simply defined and set up to include, e. g., new sensors, or debugging information, which is automatically logged, and time-tagged, on board and by the ground station. Post-processing of the logged data is done by converting it to a MATLAB typical data file format.

The data sent by EAGLE are displayed live in the *Ground Control* Graphical User Interface (GUI) shown in Figure 8a. This uses the look of typical instruments from aviation, to give the user well known representations of the current state of EAGLE. The possibility of monitoring specific variables

in real-time is shown in Figure 8b. Other views are used for general telecommands, or more specific task like engine monitoring and control.



(a) Pilot view



(b) Live plot

Figure 8: Views of the Ground Control GUI

3 NAVIGATION

This section briefly describes the navigation system designed for EAGLE. The general navigation system's architecture is first outlined, followed by the description a measurement enhancement necessary for precise navigation during tethered flight test in Section 3.3.

3.1 Navigation System Architecture

The goal of the navigation system is to provide a state solution to EAGLE's Guidance and Control functions. The solution is estimated by fusing measurements of several on-board sensors: Inertial Measurement Unit (IMU), Global Positioning System (GPS) receiver, laser altimeter and magnetometer. The set of estimated states \mathbf{x} contains position, velocity and attitude of EAGLE, along with sensor biases and scale factors.

EAGLE's tailor-made navigation system uses a modular design, with independent strapdown integration and state-filter functions. The filter estimates error quantities of the strapdown propagated solution (e. g. position error, velocity error and attitude error) as well as sensor bias errors and scale factor errors. The estimated error-states $\delta\hat{\mathbf{x}}$ are regularly fed back to correct the inertial propagator and accumulated sensor error quantities, being then reset. This is done as

$$\begin{aligned}\hat{\mathbf{x}}^+ &= \hat{\mathbf{x}}^- + \delta\hat{\mathbf{x}} \\ \delta\hat{\mathbf{x}} &\Rightarrow 0,\end{aligned}\tag{1}$$

where $\hat{\mathbf{x}}^-$ is the inertially propagated navigation solution (or *a priori* estimate) and $\hat{\mathbf{x}}^+$ is the corrected, *a posteriori*, estimate.

This modular closed-loop configuration not only offers high design flexibility but also eases the non-linearities faced by the error-state Extended Kalman filter (eEKF) by having it operate in the vicinity of the error-state origin. This is ensured by the filter reset after each feedback step. Figure 9 depicts the described architecture.

Given the vehicle's high dynamics, the navigation output is required at a high rate; Therefore, the strapdown algorithm is run at the IMU output frequency, which is 100 Hz. To ease the computational

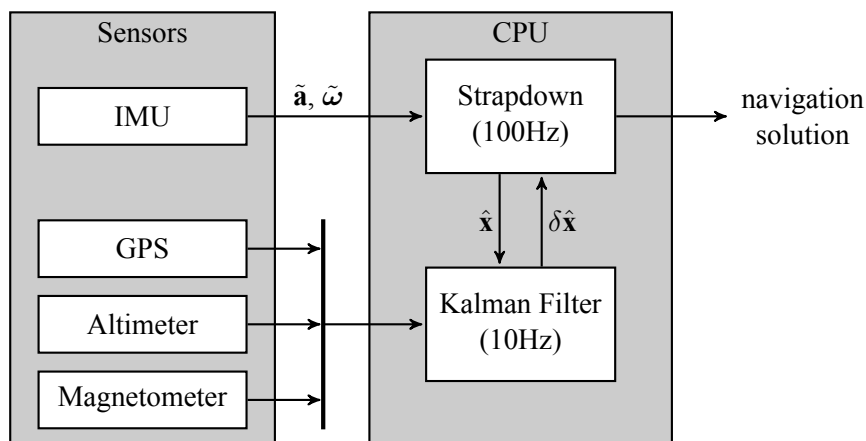


Figure 9: Navigation System Overview

effort required, the error-filter is run at a lower rate, of 10 Hz. This matches the output frequency of the remaining sensors.

An important design challenge and driver of the selected architecture is sensor output latency. While the inertial measurements of gyros and accelerometers are nearly real-time, the position/velocity fixes of the GPS receiver are often delivered with considerable delay. Depending on the receiver operation mode and options in use, this delay can be as high as 50 ms. On slow vehicular applications the entire navigation solution can be easily delayed to accommodate this latency. Under the fast-dynamics of EAGLE, however, this approach could lead to control instability. The solution found is to have the strapdown integration run in real-time while the error-state filter is delayed by 0.1 s. This method, introduced by Steffes [10], forward propagates the error-state filter estimates in order to optimally correct the real-time whole states.

3.2 Sensor Specifications

The following points describe briefly the sensors used by the navigation system of EAGLE.

- The **IMU (Inertial Measurement Unit)** includes three orthogonal single-axis gyroscopes and three orthogonal single-axis accelerometers and provides angular velocity and acceleration measurements. The employed unit is an ISIS-IMU, an advanced Microelectromechanical Systems (MEMS), with specification shown in Table 1.

Table 1: ISIS-IMU Specification

	Gyroscope	Accelerometer
Bias Stability	$< 0.05 \text{ deg s}^{-1}$	$< 10.0 \text{ mg/h}$
Scale Factor Error	$< 2000 \text{ ppm}$	$< 2000 \text{ ppm}$
Random Walk	$< 1.0 \text{ deg}/\sqrt{\text{h}}$	$< 0.05 \text{ m/s}/\sqrt{\text{h}}$

- A **GPS (Global Positioning System) receiver** provides on-board absolute positioning information in Earth Centered, Earth Fixed (ECEF) frame. The on-board receiver is able to operate in differential mode using Real Time Kinematic (RTK), being in such case connected to a second ground-fixed receiver that serves as ground station. The ground-fixed unit provides the vehicle with correction information in real-time. The airborne unit is of the *u-blox NEO-M8* series, while the ground based unit can either be of identical kind or of geodetic-grade (*Novatel ProPak*) receiver. The positioning performance (absolute and relative to the ground-station) for both standalone and differential operation (with the two ground receiver options) is shown in Table 2.
- A **Laser Altimeter** assists vertical position estimation by measuring the distance along the line of sight of the device from EAGLE to the ground. The unit used is a Micro-Epsilon optoNCDT ILR1150-10 capable of providing a range measurement from 0.5 m to 10 m with sub-centimeter accuracy.

Table 2: GPS positioning performance

Set-up	Absolute position error	Relative position error
Single, airborne unit	2.5 m	2.5 m
Differential, u-blox NEO-M8 ground-station	2.5 m	0.2 m
Differential, Novatel ProPak ground-station	0.2 m	0.2 m

- A **magnetometer** provides 3-axis local magnetic field information to support attitude estimation. The Honeywell HMC5843 unit used can measure magnetic flux density within the range of $-70\,000$ nT to $70\,000$ nT with an accuracy of 170 nT (1σ).

3.3 Visual-Aided Navigation for Tethered Test

During the tethered flight tests, EAGLE is operated at low altitude in the vicinity of buildings and other large structures. As a result, GPS satellite visibility is reduced and the impact of multi-path effects is significant. Moreover, due to the surrounding facilities, especially the tethered test frame, the magnetometer measurements also experience strong disturbances. This poses an additional challenge to the testing of the overall system. To overcome this, and provide a reliable and accurate position and attitude measurement a visual based navigation aid – the EAGLE Tag Navigator (ET-NAV) – was developed based on the AprilTags open-source software [7].

ET-NAV uses images from a low resolution (640×480) Commercial off-the-shelf (COTS) camera to identify a set of predefined marker patterns (similar to QR codes) and estimate camera position and orientation in real-time. The markers are defined such that their visual detection and recognition is performed reliably through image feature identifiers. The patterns used can be seen in Figure 20 on the right side. Since the exact location of the markers is known beforehand, as soon as relevant image features are detected and matched to these markers, the camera's position and attitude can be estimated. A Least-Squares algorithm implementation from OpenCV is used for this purpose [4]. The ET-NAV outputs are used as updates to the navigation filter. Figure 10 shows the camera and Raspberry Pi 2 computing unit used for this system. It uses an Ethernet interface to send the 10 Hz fixes to the main EAGLE navigation computer.

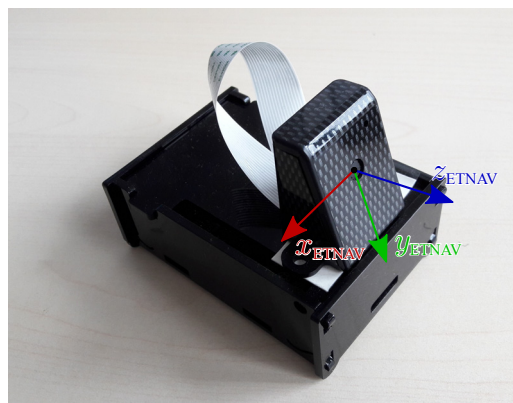


Figure 10: ET-NAV camera and computing unit overlaid with the camera reference frame

In order to correctly incorporate the ET-NAV fixes into the filter a measure of their quality (noise) is mandatory. A series of lab tests was performed having the ET-NAV camera placed on a high-accuracy rotation table, facing the marker board at different angles (see 3.4.2). From data collected, the feature detection error level could be estimated. This uncertainty information is used during flight, transformed from image pixel to position and attitude noises using the Least-Squares projection at each instant. As a way to increase the robustness of this scheme, the obtained noise covariance is calibrated online using the magnitude of the Least-Squares residuals as done in [11].

3.4 Navigation System Tests

In this section, two performance tests of the navigation system will be presented. The first test evaluates the performance of the whole navigation system on a breadboard without ET-NAV. The second test verifies only the performance of ET-NAV.

3.4.1 Navigation system evaluation

In this test, the navigation system is integrated as a navigation breadboard model as shown in Figure 11 consisting of an IMU, a GPS receiver and a laser altimeter.



Figure 11: Navigation system breadboard with dual antenna ground reference system

Ground truth of the breadboard positioning is acquired by a high-grade ProPak6 GPS receiver using both L1 and L2 frequencies and the German precise satellite positioning service, SAPOS. Additionally, accurate attitude information is provided by the receiver thanks to a dual-antenna configuration. In an optimal set-up, the accuracy of such GPS system is within 3 cm and 1 deg (given a sufficient baseline length between both antennas). However, the tests were performed in an urban-like environment where the antennas were partly shielded by buildings, leading to decreased ground truth accuracy.

Three test runs were conducted: two in which the navigation system was strapped to a cart, and one (the last) where it was hand-carried. In the beginning of each run the system was initialized for approximately 70 s to allow the internal parameters such as IMU biases and scale factors to converge. The trajectories of all three tests started and ended at the same position. The ground tracks of these tests are shown in Figure 12.

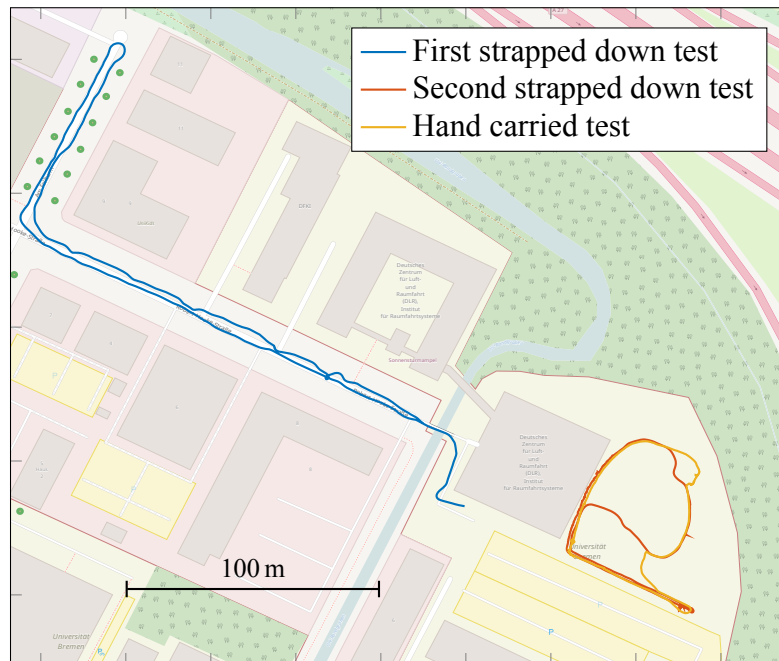


Figure 12: Ground tracks of navigation system evaluation tests

The estimated performance of the navigation system is as shown in Table 3. Note that the *open-field* performance is expected to be better than the displayed, as this was collected in sub-optimal (urban-like) conditions.

Table 3: EAGLE navigation performance

Quantity	Accuracy (1σ)	Note
Horizontal position	< 2.5 m	Based on partially-occluded GPS
Vertical position	< 0.05 m	Based on laser altimeter, for small pitch/yaw angles
Horizontal velocity	< 0.2 m s ⁻¹	Based on partially-occluded GPS
Vertical velocity	< 0.05 m s ⁻¹	Based on laser altimeter, for small pitch/yaw angles
Pitch/yaw angle	< 2 deg	
Roll angle	< 4 deg	

3.4.2 ET-NAV Tests

The performance of the ET-NAV system was evaluated both in terms of position and attitude accuracy. Prior to any testing, intrinsic calibration of the camera parameters was performed. ET-NAV position accuracy was simply checked against the range measurements of a laser altimeter. The result is in the order of 20 mm along the line of sight of the camera when placed 5 m away from the marker pattern board. Attitude testing was done using a precise three-axis rotation table having the pattern board placed in the Field of View (FoV) of ET-NAV. Two rotation sequences were carried out along the yaw and pitch axes of the camera. The measured attitude errors are plotted in Figure 13 along with the

number of detected markers. As it would be expected the attitude accuracy depends on the number of markers in the camera's FoV. For two or more detected markers the error is consistently lower than 1 deg.

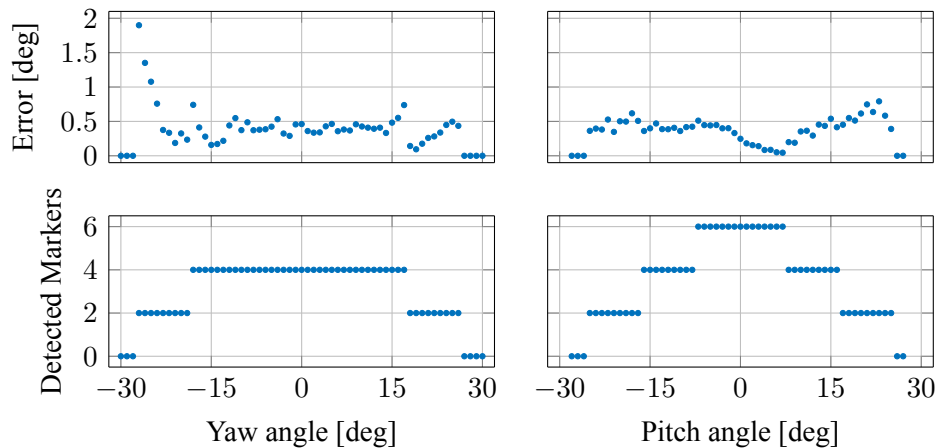


Figure 13: ET-NAV performance test around the camera axes carried out on a rotation table

4 CONTROL

The development of a control strategy for EAGLE was divided into four main phases:

- System Identification
- Roll Control
- Thrust Vector Control
- Position Control

The first phase had as goal to identify the torques and the forces that the controller can generate with the available actuators, and how accurate and reproducible they are. Moreover, it was necessary to map these forces and torques to the commands the actuators actually receive. For this purpose several experimental tests were carried out, and a series of identification strategies was conducted. The roll control has been independently developed for practical reasons: Since it is based on the use of a cold-gas system, it could be tested independently of the TVC system, and therefore was developed and validated first, and later on integrated with the thrust vector control strategy.

For the *inner loop* the control strategy is aimed at stabilizing the attitude while having EAGLE hovering at a given distance from ground, this is due to the fact that these degrees of freedom are closely related to the actuators. This development direction allows the possibility to test the attitude and altitude stabilization capabilities before having the the position control in place. Finally, the *outer loop* refers to the control activity aimed at tracking a given horizontal position. These two last degrees of freedom are indirectly controlled through the change of attitude of EAGLE and compensating for

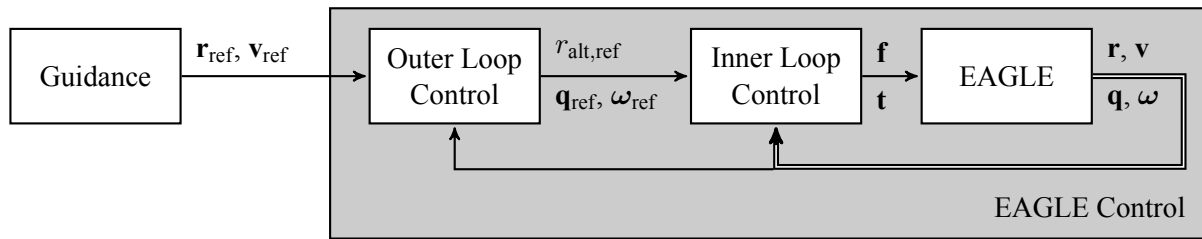


Figure 14: Control system overview

the vertical thrust loss. An overview of the control system implemented for EAGLE is depicted in Figure 14. The guidance subsystem generates the reference trajectory. The command is compared with the position and the velocity estimated by the navigation system (omitted in Figure 14 since a full description of the system can be found in Section 3). The outer loop computes a reference quaternion corresponding to the forces required for the position control. The reference quaternion \mathbf{q}_{ref} and the reference angular rate ω_{ref} are then fed to the inner loop controller which calculates the torques and forces for stabilizing EAGLE at the reference attitude.

A decision was made to develop two different strategies for the controller designs. First, a set of simple hand-tuned PD controllers was designed. These are much easier to test and verify for proper functioning than advanced controllers. These basic controllers are not further discussed within this paper.

The second strategy is based on sliding-mode control and takes the high uncertainties into account that are expected within the development of EAGLE, namely, mass, moment of inertia, alignments, etc. Figure 15 shows the different submodules implemented for the inner loop. We can distinguish the roll control, which generates the commands for the Pulse Width Modulation (PWM) logic given in milliseconds. Additionally, the TVC system acts on the pitch and yaw by deflecting the vanes, whereas the engine control is responsible for commanding the thrust force, commanded in terms of Engine Power Settings (EPS).

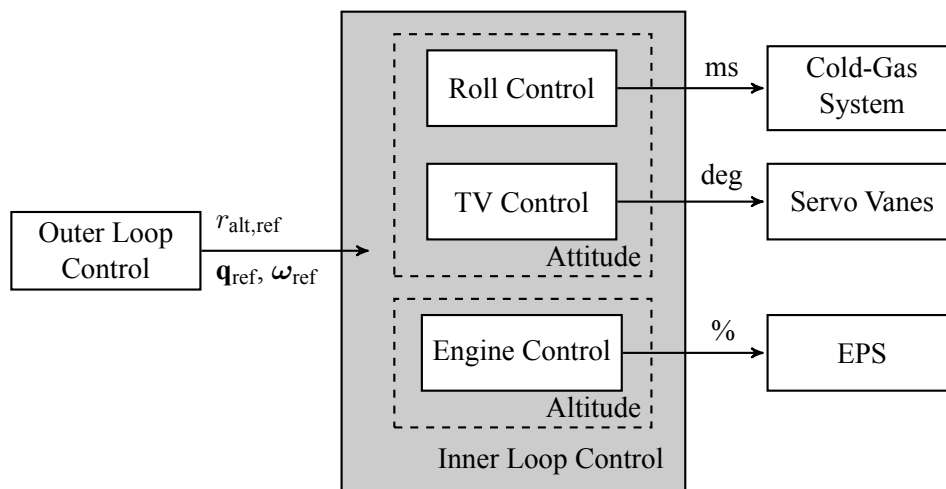


Figure 15: Inner loop architecture

The modules just referred will be described throughout this section. The identification task is described in the next section, while Sections 4.2, 4.3 and 4.4 give some information about the control structure. Note that throughout this work a very simple guidance, using set-points for the vertical and horizontal positions, has been employed. The attitude set-point is either fixed, or while the outer loop is active, it slightly varies for maneuvering EAGLE within the horizontal plane.

4.1 System Identification

In EAGLE a jet engine provides the main thrust force \mathbf{f}_{thr} , which is assumed to be generated along the x axis of the body reference frame B.

$$\mathbf{f}_{\text{thr}} = \|\mathbf{f}_{\text{thr}}\| \mathbf{e}_x^B \quad (2)$$

This reference frame has its origin in the Center of Mass (CoM) of the vehicle and is aligned with the mechanical system M. The y and z axes define the pitch and yaw axes, and are controlled through the rotation of the two TVC vanes. The B and M frames are depicted in Figure 16.

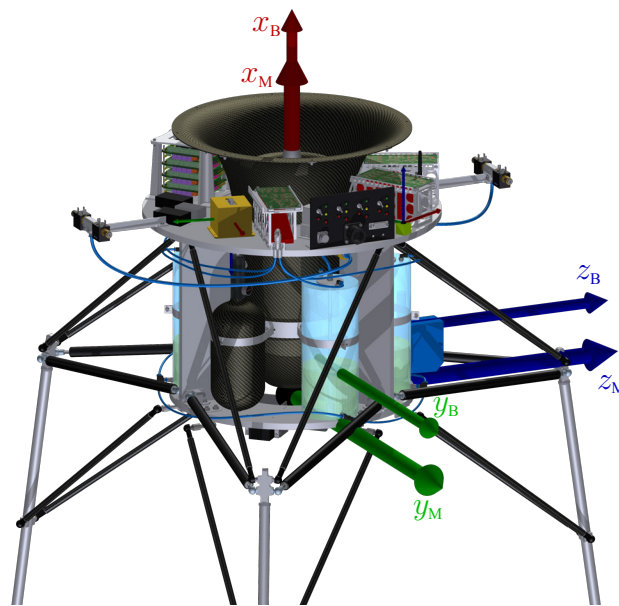


Figure 16: Mechanical reference system M and the body reference system B of EAGLE

The thrust \mathbf{f}_{thr} is mainly responsible for counteracting gravity, but parts of the main thrust can be deflected for attitude thrust vector control. The resulting force of the deflected main thrust is \mathbf{f}_{TVC} . Having the Center of Pressure (CoP) of the vanes known by construction (cf. Figure 5), and the CoM by measurement, it is possible to estimate the lever arm \mathbf{l}_{TVC} for the effectiveness of the TVC system.

The TVC force \mathbf{f}_{TVC} can be transformed into a torque \mathbf{t}_{TVC} by using

$$\mathbf{t}_{\text{TVC}} = \mathbf{l}_{\text{TVC}} \times \mathbf{f}_{\text{TVC}} \quad (3)$$

The components of the force \mathbf{f}_{TVC} can be modulated by deflecting the thrust force \mathbf{f}_{thr} by rotating the vanes. These vanes are actuated by servos s_0 and s_1 , which, together with the EPS represent the

real commands for the thrust vector control. Therefore, an identification procedure was needed to determine the mapping between commands and generated forces

$$\begin{Bmatrix} \text{EPS} \\ s_1 \\ s_0 \end{Bmatrix} \longleftrightarrow \mathbf{f}_{\text{TVC}} . \quad (4)$$

Note that the EPS is a measure of the engine's fuel pump voltage, which is the physical quantity commanded to the jet engine. The pump voltage is expressed in terms of EPS (expressed between 0 and 100) to have an intuitive way of commanding between idle thrust and full thrust.

The identification has been decomposed into two parts: First, the mapping between the EPS and the thrust force has been estimated. Secondly, for a given thrust level the TVC forces along the body axes y and z generated by deflections of the servo vanes s_0 and s_1 have been determined. The identification was carried out on a fixed test bench with EAGLE being mounted horizontally on a force-torque sensor to reduce the effects of an engine close to ground. A photograph of this set-up is given in Figure 17.

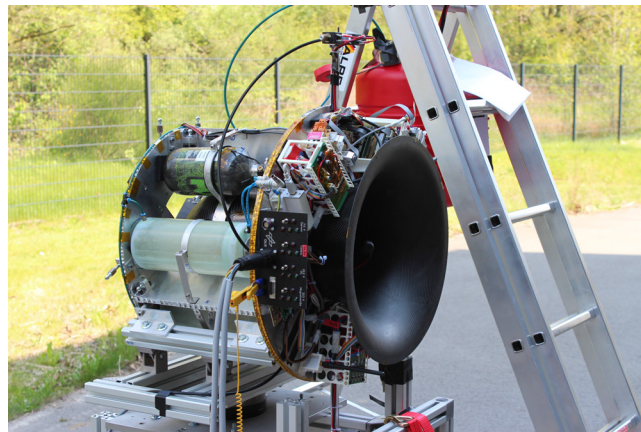


Figure 17: Test set-up for the TVC identification

For the first identification phase a cubic model has been derived from the measurements that is shown in Figure 18a. The static model was identified over multiple engine runs on different days to gain confidence on the results.

The second part focuses on the determination of the side-forces (and therefore of the corresponding attitude control torques) generated by the vanes' deflection. The tests were performed under three different thrust levels. The middle thrust is the assumed level necessary for hovering, countering the gravitational force, and an upper and lower levels: ± 30 N around hover thrust.

On each of these thrust values sequences of vane deflections were commanded focusing more on small angles, making the identification more precise in the region which is assumed important for stabilizing EAGLE. The results show that decoupled forces can be assumed for the perpendicular aligned vanes within the region of small deflection angles. Figure 18b shows the identified side force of the first vane with linear fits assuming a continuous behavior of the exhaust stream over the vane profile.

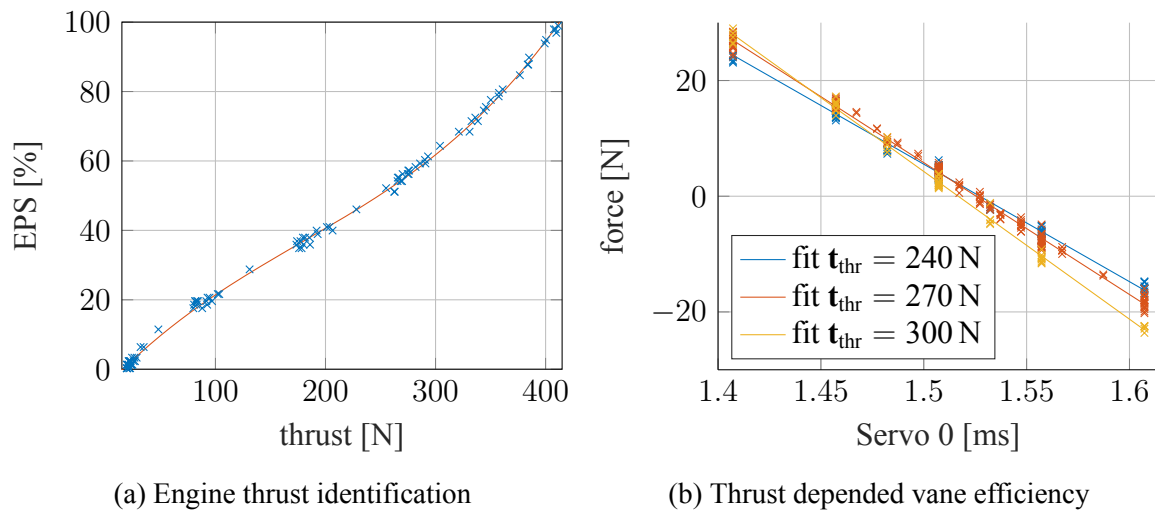


Figure 18: Identification of the TVC system

4.2 Roll Control

The cold-gas system from Section 2.1.3 controls the roll axis around the thrust direction. The roll control has to satisfy two needs: First, it has to keep the angular rate close to zero. Secondly, it has to keep a specific roll angle. Therefore, three distinct modes are defined:

- angular rate control, to ensure decoupled motion;
- minimum-time angle control, to reach a specified angle in the shortest possible time;
- angle control, which aims at keeping the roll angle at a specific value;

The cold-gas system is controlled through PWM and, therefore, a switching logic with constant period and variable pulse length has been implemented for the on-off valves. The angular rate control aims at keeping the angular rate close to zero. To include hysteresis and dead-zone in the controller, a Schmitt Trigger [12] in the command of valves is implemented. For the minimum-time roll control a minimum-time algorithm is used [5]. It is known that this algorithm provides good results in achieving the desired angle, but it is not efficient in keeping the set angle. Therefore, once that a given threshold is reached, the angle control mode is triggered. Full details about these specific algorithms can be found in [6].

4.3 Thrust Vector Control

The inner loop is also responsible for the control of the pitch angle Θ and the yaw angle Ψ , and altitude r_{alt} . A scheme for the inner loop is depicted in Figure 19.

From the depicted scheme it is possible to observe the presence of the outer loop, which computes the required reference attitude commands together with the altitude set-point. As previously mentioned, the inner loop has three separate controllers. The first is the altitude controller, which determines the thrust force to regulate the altitude of EAGLE. Then, there is the thrust vector controller,

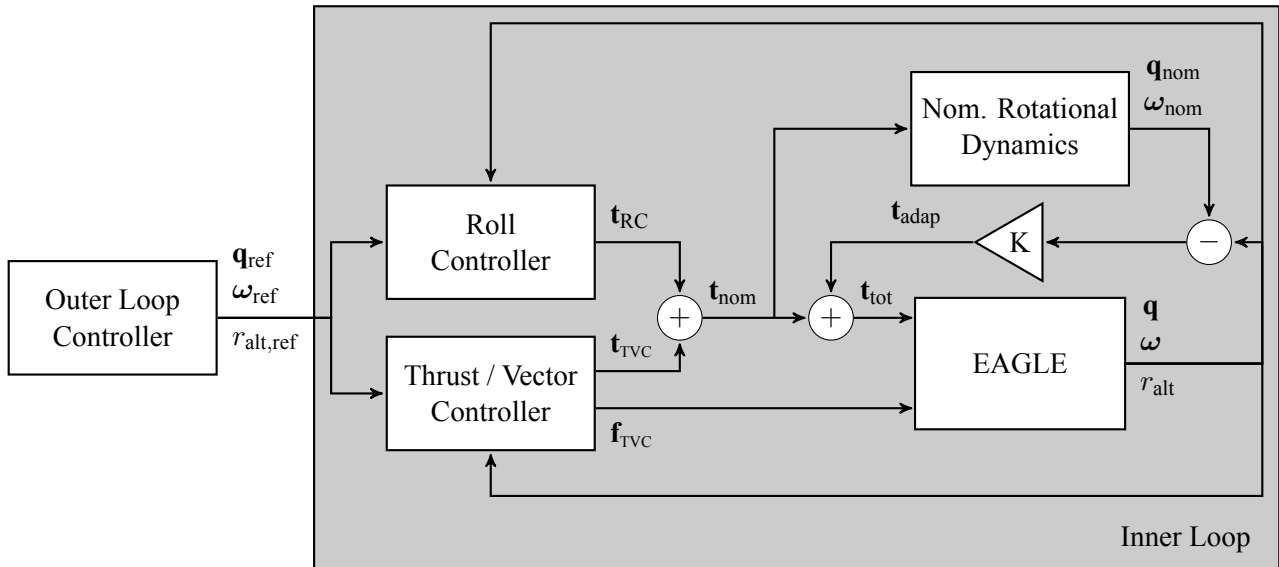


Figure 19: Inner loop detailed architecture

which is in charge of stabilizing the pitch and yaw axes; since both depend on the thrust, they are represented in Fig. 19 as one integrated block. Finally, a dedicated roll controller was implemented. As the name suggests, the roll control module stabilizes the motion around the roll axis. Additionally, a model-reference adaptive scheme has been added to make the controller able to mimic the behavior of the nominal system even in presence of significant uncertainties. However, a relevant effort has been spent to reduce these uncertainties as much as possible. The thrust controller controls the altitude dynamics such that the altitude is consistent with the reference altitude value $r_{alt,ref}$.

The control strategy is based on sliding-mode control theory [1, 8, 9]. For each of the variables to track a corresponding sliding surface s_i is designed. The sliding surfaces are of the form

$$s_i = \left(\frac{d}{dt} + \lambda_i \right)^2 \int_{t_0}^t \epsilon_i(\tau) d\tau, \quad i \in [\Theta, \Psi, r_{alt}], \quad (5)$$

where the terms λ_i are the closed-loop bandwidth of the system and ϵ_i are the tracking errors.

From the sliding surfaces it is possible to derive the non-linear control signals which bring the corresponding Lyapunov functions to zero.

$$V(s_i) = \frac{1}{2} s_i^2 \rightarrow 0, \quad i \in [\Theta, \Psi, r_{alt}]. \quad (6)$$

The sliding-mode control maps the sliding surfaces to the torques t_{TVC_y} and t_{TVC_z} and the force f_{TVC_x} which guarantee the global stability of the system.

$$\begin{Bmatrix} s_{r_{alt}} \\ s_{\Theta} \\ s_{\Psi} \end{Bmatrix} \longrightarrow \begin{Bmatrix} f_{TVC_x} \\ t_{TVC_y} \\ t_{TVC_z} \end{Bmatrix} \quad (7)$$

The torque is augmented by taking the mismatch between real plant and nominal plant into account. This is done by computing an adaptive control term, which is included in the loop, cf. Figure 19. This

adaptive part of the controller also considers the roll controller command, resulting in the total control torque \mathbf{t}_{tot} :

$$\mathbf{t}_{\text{tot}} = \underbrace{\mathbf{t}_{\text{nom}}}_{\mathbf{t}_{\text{TVC}} + \mathbf{t}_{\text{RC}}} + \mathbf{t}_{\text{adap}} . \quad (8)$$

Given the force \mathbf{f}_{TVC} and the torque \mathbf{t}_{TVC} , the actuator identification from Section 4.1 gives the vanes' deflections as well as the EPS required for the actual control of EAGLE.

$$\begin{Bmatrix} f_{\text{TVC}_x} \\ t_{\text{TVC}_y} \\ t_{\text{TVC}_z} \end{Bmatrix} \longrightarrow \begin{Bmatrix} \text{EPS} \\ s_0 \\ s_1 \end{Bmatrix} \quad (9)$$

4.4 Position Control

For the outer loop a sliding-mode control strategy was implemented too. In this case it was necessary to define two sliding surfaces for the “in-plane” components of position in the North East Down (NED) frame r_x^{NED} and r_y^{NED} . The corresponding sliding surfaces are defined as

$$s_i = \left(\frac{d}{dt} + \lambda_i \right)^2 \int_{t_0}^t \epsilon_i(\tau) d\tau , \quad i \in [r_x^{\text{NED}}, r_y^{\text{NED}}] , \quad (10)$$

where, as above, the terms ϵ_i represent the tracking errors. Since the thrust force is determined by the inner loop the sliding surfaces s_i are mapped against two side-forces f_{TVC_y} and f_{TVC_z} . The compound force given by

$$\mathbf{f}_{\text{TVC}} = \begin{Bmatrix} f_{\text{TVC}_x} \\ f_{\text{TVC}_y} \\ f_{\text{TVC}_z} \end{Bmatrix} \quad (11)$$

will be transformed into a corresponding reference quaternion $\mathbf{q}_{\text{B,ref}}^{\text{NED}}$, which will feed the inner loop. The components f_{TVC_y} and f_{TVC_z} guarantee position control in the horizontal plane. The component of the force f_{TVC_x} instead provides the hovering capability. The three components define the orientation that the body must have to track the reference position. The difference of orientation between the force vector so defined and the reference force vector is transformed into a quaternion, which represents the reference attitude to be tracked by the inner loop.

$$\mathbf{f}_{\text{TVC}} \longrightarrow \mathbf{q}_{\text{B,ref}}^{\text{NED}} \quad (12)$$

Note that the closed-loop bandwidths $\lambda_{f_{\text{TVC}_y}}$ and $\lambda_{f_{\text{TVC}_z}}$ are quite smaller than the ones used for the inner loop, that is λ_{Θ} and λ_{Ψ} . This is done to separate the two loops to a point where the inner loop is significantly faster in stabilizing EAGLE, and the inner dynamics can be neglected during the design of the outer loop.



Figure 20: Tethered Flight Test Facility

5 TETHERED FLIGHT RESULTS

The first tests of EAGLE were conducted within a safe environment. This Tethered Flight Test Facility was designed to safely handle EAGLE during the first hovering tests, but also for later tests when EAGLE's software or hardware were modified and a safe operation could not be guaranteed prior to the test. The current status of the facility is depicted in Figure 20.

Within this test set-up we proved the feasibility of hovering EAGLE within a small confined space applying a high standard for the safety of EAGLE as well as personnel and observers. At the same time it allows a quick access to the lander for conducting consecutive tests with a short turn-around-time.

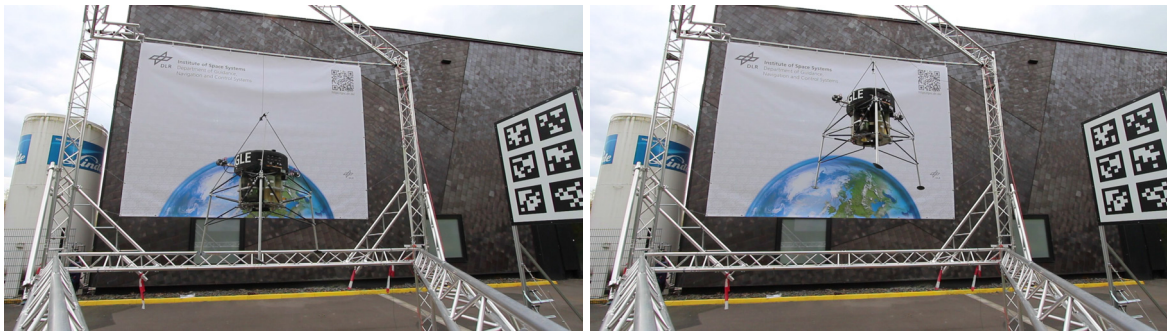
Depending on the maturity of the overall system, different ways of tethering EAGLE are possible. The picture shows the set-up with only a single tether to the top of the vehicle which is used if the GNC system is already reliable. The tether is connected to a rubber band dampening jerks during lift-off and landing, and in unforeseen situations, when the tether is stretched.

Three separate tests were conducted to prove the functioning of the individual controllers for altitude (5.1), roll (5.2), and position (5.3). During these tests all controllers were active, but the set-point for only one controller was changed at a time.

5.1 Altitude controller

This section shows the first performance test of the sliding-mode altitude controller that was discussed in Section 4.3. The performance of this controller is expected to improve in the future, but the results show that the current maturity level is sufficient to stabilize the altitude of EAGLE.

Due to the fact that the space where EAGLE can move freely within the tethered flight facility is restricted, the altitude controller is tested within a range of 0.5 m to 1.2 m only. The dynamic behavior



(a) Lower bound of the clearance

(b) Upper bound of the clearance

Figure 21: The altitude bounds for EAGLE during the sliding-mode altitude controller test

below 0.5 m is heavily disturbed by the tether which is pulled up by the rubber band. The upper limit is defined by the visibility of the tag board from ET-NAV. Figure 21 shows these limits captured during the test.

Within these limits EAGLE was commanded to different set-points of altitude to evaluate the performance and control quality of the new controller. Figure 22 shows the data recorded during the test. The upper plot shows the commanded and measured altitude over the test cycle, the negative sign comes from the *down* direction from the chosen NED reference frame. The climb and descent cycles, and stationary flights follow the set-point commanded by the ground station. The control error (depicted in the lower plot) clearly shows a general constant offset that is smaller than 20 cm.

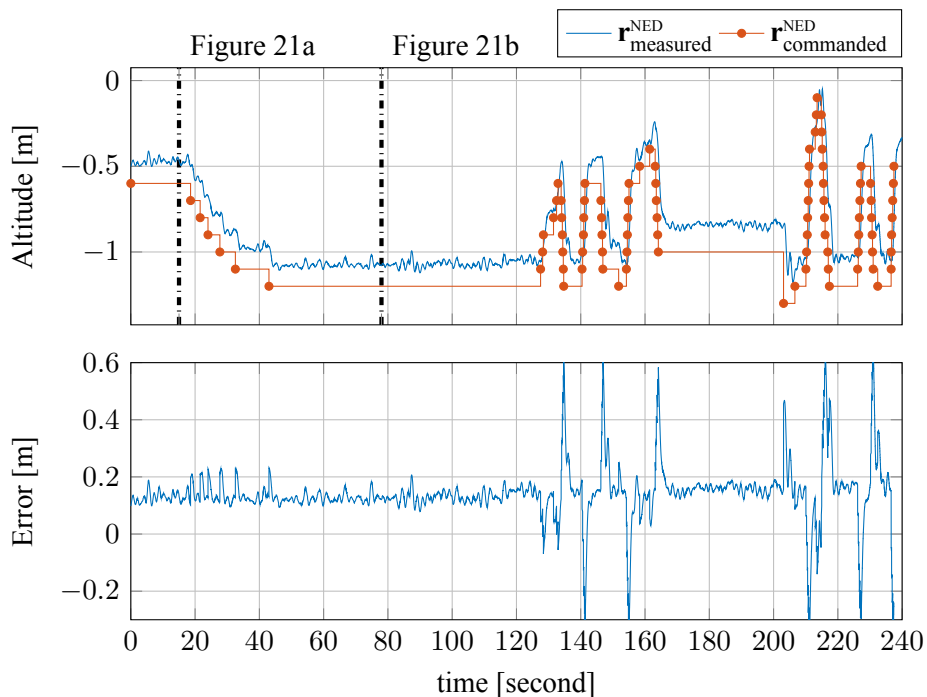


Figure 22: Altitude control - sliding mode control

The visible spikes result from the dynamics of EAGLE. When a new set-point is issued the error instantaneously grows and, in the following seconds, the relatively slow engine thrusts up (or down) to maneuver EAGLE to the new position reducing the error.

There are probably multiple reasons for the constant offset. First, the sliding-mode controller was tuned conservatively. Additionally, for the initial test campaign it was decided to suppress the integral part of the controller (resembling a PD controller) to avoid problems coming from a saturating integrator of a sub-optimally tuned controller. Furthermore, the magnitude of the control deviation is largely dominated by the feed-forward part, that roughly acts as gravity compensation. This feed-forward contribution assumes a well identified engine thrust and a known mass that is changing over time. Both requirements are only known with large uncertainties, resulting in the given deviation from the set-point.

The flight test showed a working sliding-mode altitude controller. The performance will increase in the future by refining the parameter tuning, and allowing for a stronger action of the non-linear part of the controller. Eventually, better estimates for the physical characteristics of EAGLE, such as Mass, Center of Mass, Inertia (MCI), actuator identification, etc., will also improve the overall controller performance.

5.2 Roll controller

The RCS for the roll axis of EAGLE had already been successfully tested within a lab environment as stated in Section 4. It was an advantage during early flight tests to have a control system safely stabilizing the roll axis, as focus focus could be put on the other axes. After, the overall control system was tested the roll controller also had to prove its capabilities during a simple slew maneuver, where EAGLE was commanded a series of roll angle set-points. The commands and the resulting measured attitude are shown in Figure 23. EAGLE follows the quick succession of commands gracefully and generally reduces the control error within 0.4 s. The quick cold-gas actuator and the variable pulse length enable a rapid and precise roll control.

5.3 Position controller

The most challenging controller verification is for the horizontal position control. A working position control relies on a working inner loop, and so outer and inner loop are tuned to work together. Resulting from the thrust vector control configuration, EAGLE is a non-minimum phase system with respect to position control. The first test showed a position control accuracy of ± 0.2 m and a very slow reaction under changing set-points. In Figure 24 the results are shown for the North and East direction vs. time (left), and within the horizontal North-East plane (right).

In the individual time series plots it can be seen that EAGLE follows the commanded position with a delay of about 10 s, defining a rectangular ground track with the dimensions of 0.5 m by 1.0 m. By performing a further refinement of all the underlying controllers within the inner loop, an increase in the position tracking is expected. However, in free flight the navigation solution will be based on a GPS RTK receiver, and therefore not significant improvements in positioning accuracy with respect to the already demonstrated figures are expected. For this reason, further development will focus on a faster convergence to the set-point rather than steady-state accuracy.

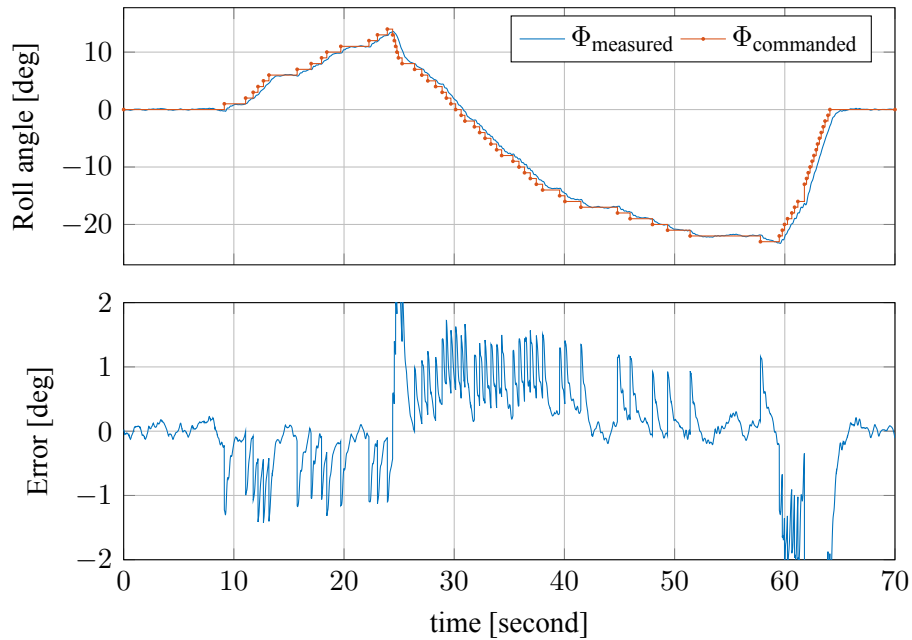


Figure 23: Roll control

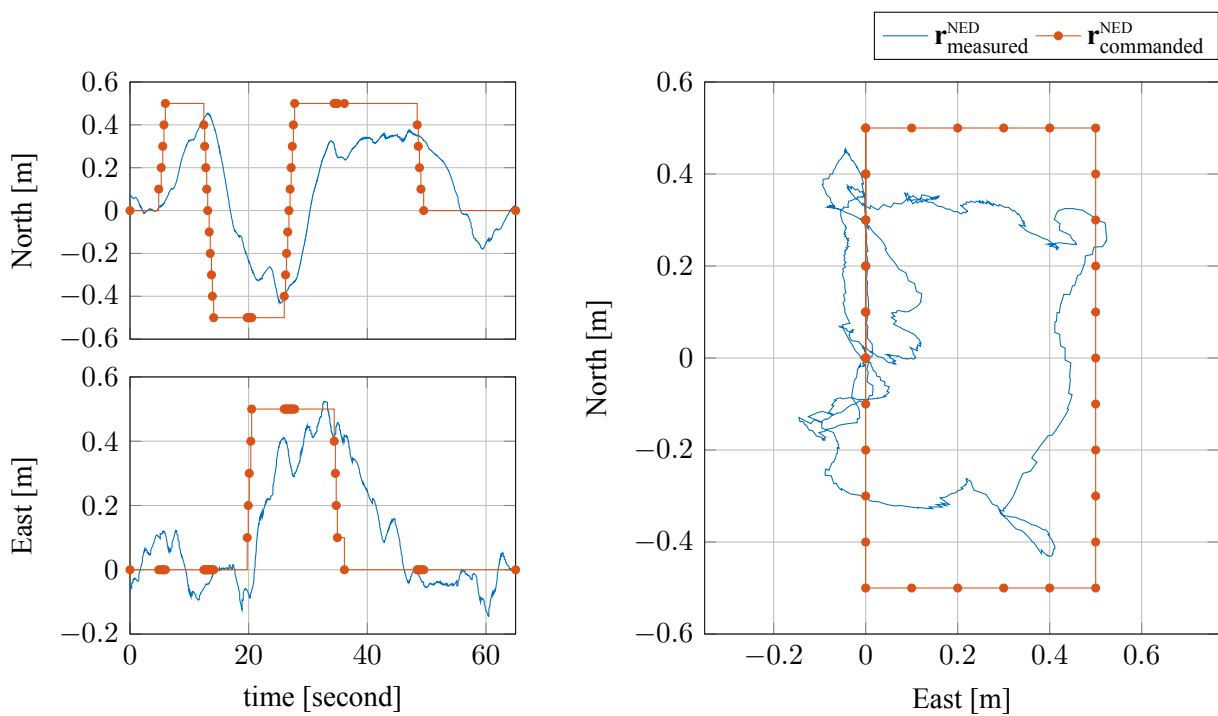


Figure 24: Position control

6 CONCLUSIONS AND OUTLOOK

This paper presented the design and status of EAGLE as a test environment for GNC systems. Flight test results have been presented showing the suitability of the vehicle for rapid development and testing.

The vehicle and system are relatively easy to handle. It supports rapid-prototyping for GNC functions based on Matlab/Simulink code generation. After test planning and software updating, the preparation of the vehicle as well as its rigging to the tethered flight test facility takes only a very short time, making it possible to perform several flight tests on a single day.

So far, EAGLE successfully demonstrated hovering with position control. The immediate next steps are lift-off from ground and landing on ground. Additionally, other settings and algorithms for guidance and control will be implemented and tested.

Another major step is conducting free (untethered) flights. For that a few more logistical and administrative steps have to be completed in order to get access to a test range with a restricted air space and to obtain the corresponding flight permissions. Of course, the highest possible confidence in the system has to be achieved with more tethered flight tests.

In parallel, two currently on-going studies at Deutsches Zentrum für Luft- und Raumfahrt (DLR) explore different options to extend the existing system. The first study focuses on creating a larger version “EAGLE XL” which uses a larger jet engine as the main thruster, e. g. an engine with a nominal thrust of 1500 N. Since the larger engine is more fuel efficient and many of the subsystems do not scale one-to-one with the size of the engine this version would allow for either more payload or more fuel mass enabling more flight time and a larger flight envelope.

A second study focuses on replacing the jet engine with a set of green mono-propellant rocket engines. This configuration would go beyond the pure testing of GNC and would allow to gain test results and handling experience with a propulsion system which is very similar to planetary landers or returning first stages with a powered landing.

The test vehicle EAGLE is available to the community as part of joint research projects and studies. For instance, it will be employed within the ESA NPI “Advanced Flight Control System Design with Active Load & Relief Capabilities” under ESA contract no. 4000119571/17/NL/MH in collaboration with University of Bristol and Airbus Defense and Space Germany.

7 ACKNOWLEDGMENTS

The development and implementation of EAGLE is an internal project of the Institute of Space Systems of DLR. The final phase was supported as part of the project “Upper Stage Attitude Control Design Facility (USACDF)” under subcontract of Airbus Defense and Space Germany and the European Space Agency.

REFERENCES

- [1] B. Fernandez and K. J. Hedrick. “Control of Multivariable Non-Linear Systems by the Sliding Mode Method.” In: *Int. J. Control*, Vol. 46, No. 3, pp-1019-1040 (1987).

- [2] C. Gu, S. Heynen, and T. Poirrier. “HOMER Take-off: A Review.” In: *dSPACE Magazine* 2015.2 (June 2015), pp. 32–35.
- [3] C. Gu, P. Vernis, J.F. J.F. Jourdas, N. Hachelef, S. Heynen, T. Poirrier, A. Schwientek, and O. Boudillet. “HOMER PROJECT: Development, validation, qualification and flight test results of the autonomous flight control of the test vehicle.” In: *9th International ESA Conference on Guidance, Navigation & Control Systems*. June 2014.
- [4] Itseez. *Open Source Computer Vision Library*. <https://github.com/itseez/opencv>. 2015.
- [5] D. E. Kirk. *Optimal Control Theory - An Introduction*. Dover, 1970. isbn: 978-0486434841.
- [6] W. C. Leite Filho, M. Dumke, and Theil S. “Control System Design of the Lander Demonstrator EAGLE.” In: EUCASS. 2015.
- [7] E. Olson. “AprilTag: A robust and flexible visual fiducial system.” In: *Proceedings of the IEEE International Conference on Robotics and Automation (ICRA)*. IEEE, May 2011, pp. 3400–3407.
- [8] W. Perruquetti. *Sliding Mode Control in Engineering*. Marcel Dekker Inc, 2002.
- [9] Y. B. Shtessel, C. Edwards, L. Fridman, and A. Levant. *Sliding Mode Control and Observation*. Birkhäuser, 2013.
- [10] S. R. Steffes. “Computationally Distributed Real-Time Dual Rate Kalman Filter.” In: *Journal of Guidance, Control and Dynamics* (2014).
- [11] S. Urban, J. Leitloff, and S. Hinz. “MLPnP - A Real-Time Maximum Likelihood Solution to the Perspective-n-Point Problem.” In: *The ISPRS Annals of the Photogrammetry, Remote Sensing and Spatial Information Sciences* (2016).
- [12] B. Wie. *Space Vehicle Dynamics and Control*. AIAA Education Series. American Institute of Aeronautics and Astronautics, Inc., 2008. isbn: 978-1-56347-953-3.